

The island wind–buoyancy connection

By AGATHA M. De BOER[†] and DORON NOF^{*‡}, *Department of Oceanography, Florida State University, Tallahassee, 32306-4320, USA*

(Manuscript received 19 February 2004; in final form 7 March 2005)

ABSTRACT

A variety of recent studies have suggested that the meridional overturning circulation (MOC) is at least partially controlled by the Southern Ocean (SO) winds. The paradoxical implication is that a link exists between the global surface buoyancy flux to the ocean (which is needed for the density transformation between surface and deep water) and the SO winds. Although the dependency of buoyancy forcing on local wind is obvious, the global forcings are usually viewed independently with regard to their role as drivers of the global ocean circulation. The present idealized study is focused on understanding this wind–buoyancy connection. In order to isolate and investigate the effect of SO winds on the overturning we have neglected other important key processes such as SO eddies.

We present the wind–buoyancy connection in the framework of a single gigantic island that lies between latitude bands free of continents (such as the land mass of the Americas). The unique geometry of a gigantic island on a sphere allows for a clear and insightful examination of the wind–buoyancy connection. This is because it enables us to obtain analytical solutions and it circumvents the need to calculate the torque exerted on zonal sills adjacent to the island tips (e.g. the Bering Strait). The torque calculation is notoriously difficult and is avoided here by the clockwise integration, which goes twice through the western boundary of the island (in opposite directions) eliminating any unknown pressure torques.

The link between SO winds and global buoyancy forcing is explored qualitatively, using salinity and temperature mixed dynamical-box models and a temperature slab model, and semiquantitatively, employing a reduced gravity model which includes parametrized thermodynamics. Our main finding is that, in all of these cases the island geometry implies that the stratification (and, hence, the air–sea heat flux) can always adjust itself to allow the overturning forced by the wind. We find that, in the mixed dynamical-box models, the salinity and temperature differences between the boxes are inversely proportional to the MOC. In spite of the resulting smaller north–south temperature difference, the meridional heat transport is enhanced.

1. Introduction

Traditionally, meridional overturning has been regarded as a large-scale flow driven solely by the surface heat and fresh-water fluxes. Hence, it was originally called the thermohaline circulation. In a groundbreaking study, Toggweiler and Samuels (1993, 1995) challenged this view by revealing a strong correlation between North Atlantic Deep Water (NADW) formation and winds over the Southern Ocean (SO). Since then, numerous models have corroborated this connection, albeit with varying sensitivity (McDermott, 1996; Rahmstorf and England, 1997; Nof, 2000, 2002, 2003; Bjornsson and Toggweiler, 2001; Klingler et al., 2003).

Of course, this new and unexpected facet of the overturning presents only an additional piece to the puzzle that is the large-scale ocean circulation. We know that deep water cannot form if the surface water is too cold or too fresh, regardless of what the SO winds do. However, the above numerical studies indicate that, to a large extent, the ocean can adjust its temperature and salinity distribution over time to allow the overturning that the SO winds prescribe. In this paper, we address the question of how this adjustment can take place. We do so using a single gigantic island on a sphere; this allows us to examine the problem analytically. We see that, even though in our model the meridional overturning circulation (MOC) is determined by the wind, the oceanic stratification adjusts itself in such a manner that the supposedly independent buoyancy force can always cause the surface-to-deep-water conversion imposed by the wind.

1.1. Background

The importance of the SO winds lies in the fact that they blow over a latitudinal belt of the ocean that is free of continents.

[†]Corresponding author.
e-mail: adeboer@princeton.edu

^{*}Current affiliation: Atmospheric and Oceanic Sciences Program, GFDL/Princeton University, PO Box 308, Princeton, 08540, USA

[‡]Additional affiliation:
Geophysical Fluid Dynamics Institute, Florida State University.

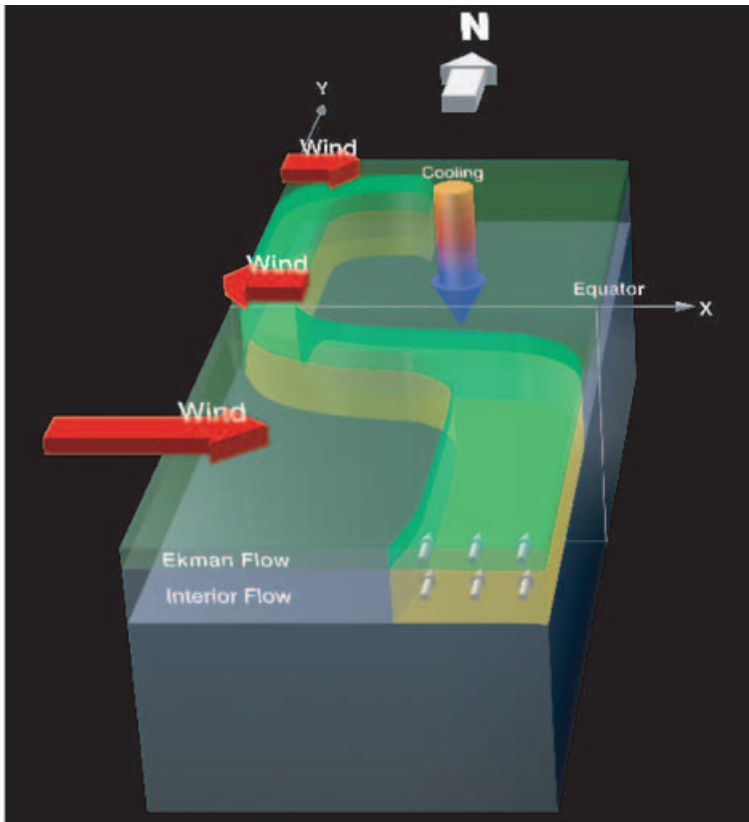


Fig 1. The three-dimensional path of SO water to the northern basin. Even though the total amount of water transported northward in the SO is identical to the Ekman flux there, most of the water that constitutes the S-shaped path corresponds to interior geostrophic flow along the eastern boundary and not to the southern Ekman flux (reproduced from Nof and De Boer, 2004).

Not only are these winds very strong (due, partly, to the lack of surface topographic obstacles) but, more importantly, the open latitude belt ocean dynamics is fundamentally different from that of bounded ocean basins (Gill and Bryan, 1971). A net geostrophic meridional flow is prevented by the open channel which encompasses the entire globe. Consequently, to conserve mass, an amount of water equal to the northward-driven Ekman flow must either return through non-geostrophic eddy fluxes (Gnanadesikan, 1999; Speer et al., 2000; Sloyan and Rintoul, 2001) or sink below topography, where it can return southward in geostrophic balance. A good overview of the relative importance of these two return pathways is provided by Rintoul et al. (2001). Some of the sinking may occur in the South Atlantic (SA) and South Pacific in the Deacon cell (Döös and Webb, 1994; Döös, 1994), but a significant portion sinks in the North Atlantic (NA), where known regions of deep convection exist. It is important to realize that it is not the southern Ekman water itself that crosses the equator and later sinks to the deep ocean in the NA, but rather the Sverdrup interior water (Nof, 2003; Nof and De Boer, 2004; see Fig. 1). This will become apparent later when our results are discussed.

Recently, Wunsch (2002) has pointed out that the term ‘thermohaline circulation’ is a misnomer because surface buoyancy fluxes alone cannot provide the energy needed to overturn a stratified ocean. He instead suggested the use of the name ‘meridional overturning circulation’ for the over-

turning of mass for which tidal and wind energy is required (rather than buoyancy forcing alone). The inability of the heat and freshwater fluxes to overturn the ocean without southern ocean upwelling of deepwater is manifested in the ‘missing mixing’ problem (Webb and Sugimotohara, 2001). In the conventional picture of the conveyor belt (Broecker, 1987), the upwelling can occur through downward mixing of heat in low latitudes (Munk, 1966), but observational evidence indicates that diapycnal mixing in the thermocline is insufficient to close the circulation budget (Ledwell et al., 1993; Polzin et al., 1995; Ledwell et al., 1998; Law et al., 2003). In the alternative scenario of an overturning driven by strong southern winds, the upwelling can occur in the SO through wind divergence. Toggweiler and Samuels (1998) found that such a wind-driven overturning circulation can exist without vertical mixing, provided that an Antarctic circumpolar channel is present. Furthermore, using a new tracer method, Döös and Coward (1997) found that most of the NADW upwells in the SO, and this was also corroborated by the inverse model of Sloyan and Rintoul (2001). The tracer budget study of Ganachaud and Wunsch (2000) indicates much higher vertical mixing (in the range of $3 \times 10^{-4} \text{ m}^2 \text{ s}^{-1}$ to $12 \times 10^{-4} \text{ m}^2 \text{ s}^{-1}$), although this is predominantly in the deep ocean. Surface upwelling also occurs in their inverse model in the SO. Other related works that concern the SO winds and mixing in the SO are those of Gille (1997), Stevens and Ivchenko (1997), Tsujino and Sugimotohara (1999), Karsten et al.

(2002), Greatbatch and Lu (2003) and Naveira Garabato et al. (2004).

In this study, for simplicity, we neglect eddy fluxes in the SO and assume a one-to-one relation between the SO winds and the MOC. By MOC, we mean the water that flows northward at the southern island tip, sinks somewhere east of the island and then returns to the SO below the topography (at the Drake Passage latitude). We purposely keep the definition of our MOC broad because our models are not suited to distinguish between different regions of sinking. In the real ocean (and in numerical models) some of the northward-driven flow sinks in the NA, a portion returns back south in the Deacon cell (via isopycnal flows) and the rest returns above the topography through eddy fluxes. In this study, we are concerned with all sinking that requires buoyancy transformation. The numerical results which indicate a link between SO winds and NADW formation (Toggweiler and Samuels, 1995; McDermott, 1996; Rahmstorf and England, 1997; Nof, 2000, 2002, 2003; Bjornsson and Toggweiler, 2001; Klinger et al., 2003) together with the arguments against a purely thermodynamically driven overturning circulation (and the requirement for wind energy) indicate that the wind–overturning relationship represents an important part of the dynamics of the real ocean. As such, it deserves to be studied in isolation, although it should be kept in mind that it represents only a part of the problem.

1.2. This study

In Section 2 we formally derive the meridional overturning associated with a gigantic island on a sphere (Fig. 2) using what we call the ‘Belt Constraint’. This is an expression for the transport across a latitudinal belt free of continents in terms of the zonal wind field at that latitude. The Belt Constraint is taken to represent the upper limb of the MOC. In reality, it only constrains the northward flow at the southern tips of the continents (in an eddy-free ocean) and does not provide information on the flow path or sinking regions. Again, our neglect of SO eddies or sinking regions other than those in the NA does not reflect a view that these processes are unimportant. The relative importance of all the processes that determine the MOC remains enigmatic and we do not attempt to quantify them here. Rather, we isolate the dynamics related to the SO winds and NADW formation in order to understand the thermodynamic mechanism that connect them to each other.

The one-island geometry is chosen to resemble, for example, the land mass of the Americas (Fig. 3) and to give a simple enough problem which would enable us to examine the processes in detail. A more realistic depiction would have been two large islands, where the second represents the Africa–Eurasia continents (Nof, 2002). Actually, any geometry that leaves at least one open latitude band free of continents will be subject to a wind-driven overturning and, therefore, reveal the wind–buoyancy connection. Nevertheless, we prefer to address the case

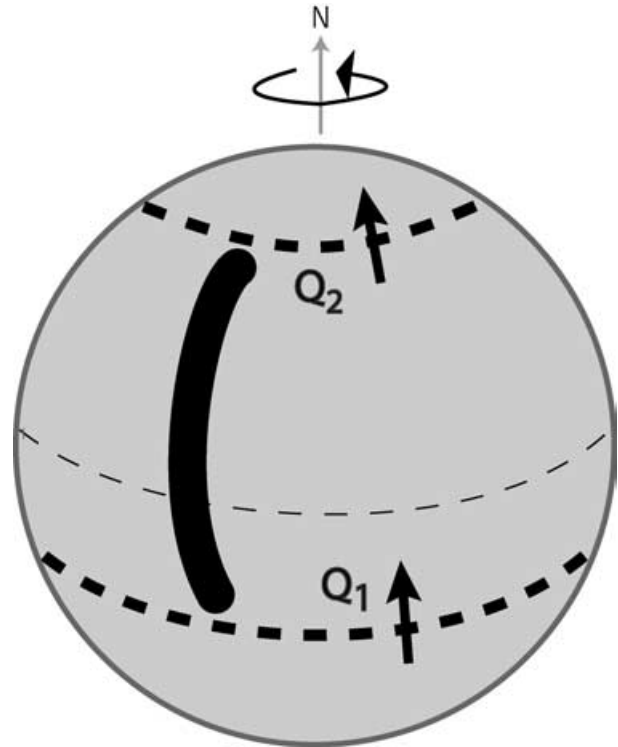


Fig 2. A single meridional island on a sphere. $Q_{1,2}$ are the wind-forced transports (in the upper layer, above topography) across the southern and northern belts, respectively. For $Q_1 - Q_2 > 0$ there must be a net sink between the island tips. The island represents the Americas or the Africa–Eurasia continents.

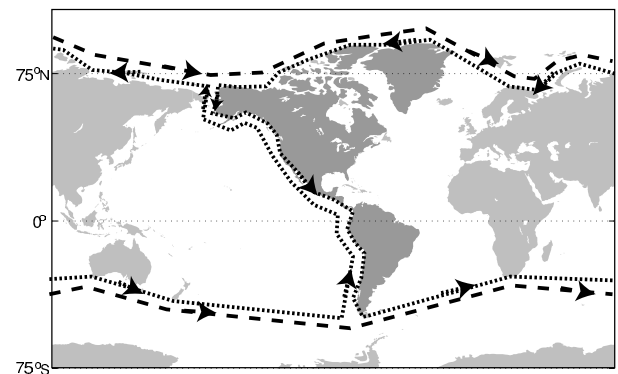


Fig 3. The continents of the Americas are chosen here to illustrate the IR for a gigantic island on a sphere. The dotted line is the wind integration contour for the IR and the dashed lines are the contours used for the belt constraints. Because the Americas are chosen to resemble a single island on a sphere, the integration path does not follow the eastern boundary of Africa and Europe (as in Nof, 2002). Note that, even though the Bering Strait is only 50 m deep, the sections of the IR integration path along the eastern boundary of the Americas cancel so that the pressure drop across the strait is irrelevant.

of one island because it is simple, can be dealt with analytically, and is sufficient to elucidate the wind–buoyancy question. The MOC derived from the Belt Constraint is shown to be consistent with Godfrey’s original Island Rule (IR) when sinking is accounted for between the island tips (Godfrey, 1989; Pedlosky et al., 1997; Firing et al., 1999; Stanton, 2001).

Next, we show that the ocean aligns the global buoyancy forcing to the SO wind forcing by adjusting its stratification. In Section 3, this is shown conceptually with the use of a salinity and temperature box model and a temperature slab model. In Section 4, a reduced gravity model, adapted to include buoyancy forcing, is used to illustrate the stratification adjustment numerically. We discuss our results in Section 5 and present our main conclusions in Section 6.

2. The Belt Constraint and the wind–buoyancy connection

Consider a single meridional elongated island on a sphere (Fig. 2). The net north–south transport across the zonal contours passing through the island tips can be derived analytically as follows. We integrate the linearized Boussinesq momentum equations for a continuously stratified fluid from the surface to a fixed depth, H , below the Ekman layer (so that the stress is zero) and above the bottom topography,

$$-\rho_0 f V = -\frac{\partial P}{\partial x} + \tau^x, \quad (1)$$

$$\rho_0 f U = -\frac{\partial P}{\partial y} + \tau^y - RV, \quad (2)$$

where ρ_0 is the mean density, f is the Coriolis parameter and U and V are the depth integrated zonal and meridional velocity, respectively. P is the depth integrated pressure (from the surface to H , a predetermined depth which is not necessarily a level of no motion and is slightly above topography) and τ^i is the surface wind stress in the i direction. Note that, for clarity, all variables are defined in both the text and the Appendix. Equations (1) and (2) correspond to a Sverdrup interior and frictional western boundary currents. Most of the energy dissipation occurs in the western boundary region through the term RV (where R is a frictional parameter). Integrating eq. (1) zonally around an open latitude band free of continents eliminates the pressure term so that

$$Q_i = -\frac{\oint_i \tau^x dx}{\rho_0 f_i}, \quad (3)$$

where Q_i is the transport across the integration path, i , from the surface to H . For the remainder of this paper we refer to eq. (3), previously derived by Nof (2003), as the Belt Constraint.

Again, it is emphasized that, even though eq. (3) looks like and must necessarily be equal to the Ekman transport, it corresponds to the water mass associated with the Sverdrup transport along the eastern side of the basin rather than the Ekman flux itself.

This point is subtle and we will explain it further. In a strictly mathematical sense, the Belt Constraint must be equal to the Ekman transport because it is the net flow across a closed latitudinal integration path where at any depth below the Ekman layer the integrated geostrophic transport must be zero. However, in the sense that eq. (3) represents northward flowing water that sinks to depths below the ‘Drake Passage’ topography, it does not correspond to the surface water in the Ekman layer. The water that will eventually reach the NA to sink there enters the SA on the east through the Sverdrup interior. In fact, the actual water mass that returns southward at the latitude of the Belt Constraint may never have been in the Ekman layer at that latitude. Consider further that, if it is strictly the Ekman layer water that represents the upper limb of the meridional overturning cell, then the sinking in the Pacific must necessarily be twice as strong as in the Atlantic, a fact which we know to be false. This issue is discussed in detail in Nof (2003) and Nof and De Boer (2004).

The amount of water that converges between the tips of the island in Fig. 2 can now readily be derived from the Belt Constraint (3),

$$W = Q_1 - Q_2, \quad (4)$$

where the subscripts 1 and 2 refer to the southern and northern tips, respectively. Steady-state conditions require that an amount of water, W , sink below H and return to its origin. We assume adequate bottom topography at the latitude of the island tips to enable a geostrophic return flow at depth.

Therefore, the wind drives a meridional overturning that requires sinking and rising of water (to connect the opposing surface and deep flows). In a stratified ocean, large vertical excursions are accompanied by buoyancy transformations. The density changes are facilitated by surface heat and freshwater fluxes. Herein lies a paradox. There is no known direct relation between the strength of the SO winds and the global buoyancy forces. Traditionally, wind and surface buoyancy fluxes have been regarded as independent forces, but the above example indicates that they must be aligned. The main purpose of this study is to investigate this connection.

Before continuing, we briefly show that the current geometry highlights a problem in the application of Godfrey’s IR (Godfrey, 1989) to large islands and how this can be corrected. Our starting point is again the horizontal momentum equations. We integrate eq. (1) along AB and CD (see Fig. 4) and eq. (2) along BC and DA. Adding the four resulting equations yields

$$\rho_0(-f_1 Q_1 + f_2 Q_2) = \oint \tau^r dr, \quad (5)$$

where, again, the subscripts 1 and 2 refer to the southern and northern island tips so that $Q_{1,2}$ are the transports across AB and CD, respectively. The integral $\oint \tau^r dr$ is the counterclockwise integrated wind stress along the path. Because the frictional term RV is of $O(1)$ only in the western boundary region (which we avoid in this integration), it does not enter the rest of the

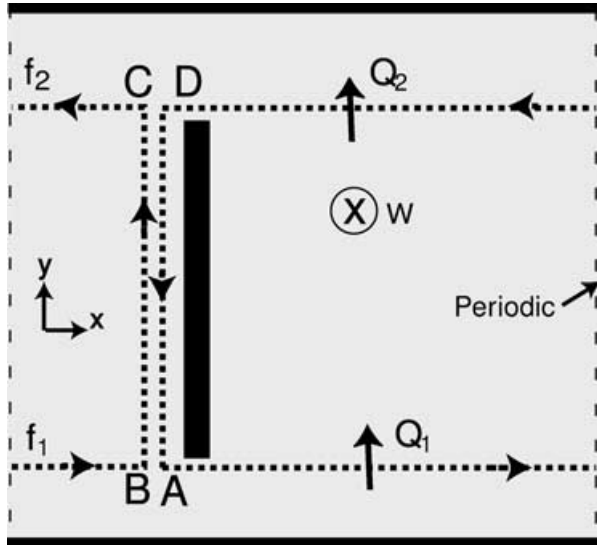


Fig. 4. Top view of a zonally periodic ocean basin. The thick dashed contour shows the integration path (ABCD) for an island on a sphere. The thin dashed line indicates the periodic boundaries. $Q_{1,2}$ are the transports across AB and CD, respectively, and $f_{1,2}$ are the Coriolis parameters at the island tips. The downwelling, W , is indicated by \otimes .

problem. In the original derivation of the IR, a level of no motion is assumed and the flow around the island is taken to be non-divergent. Setting $Q_1 = Q_2$ then gives the results

$$Q_1 = Q_2 = \frac{\oint \tau^r dr}{\rho_0(f_2 - f_1)}. \quad (6)$$

Clearly, eq. (6) is not reconcilable with the application of the Belt Constraint (3) at the two island tips. The reason is that it does not account for sinking/rising of water in the basin adjacent to the island. Vertical fluxes are always present next to large islands but essential in the current geometry. To overcome this problem we introduce a term $W = Q_1 - Q_2$ to represent the vertical mass exchange between the upper and lower layers east of the island. Solving for Q_1 and Q_2 in terms of W gives the desired adjusted IR:

$$Q_1 = \frac{\oint \tau^r dr + \rho_0 f_2 W}{\rho_0(f_2 - f_1)}, \quad (7)$$

$$Q_2 = \frac{\oint \tau^r dr + \rho_0 f_1 W}{\rho_0(f_2 - f_1)}. \quad (8)$$

Substitution of eqs. (3) and (4) into eqs. (7) and (8) reveals that the Belt Constraint and IR are now consistent. Note, however, that they do not describe the same physics. Our thermodynamic IR is under constrained; it consists of only two equations (eqs. 7 and 8) but three unknowns (W , Q_1 and Q_2). Only explicit use of the periodicity at the island tips produces the additional constraint to uniquely solve the problem. In addition, the thermodynamic IR can be applied to any island, while the belt constraint requires

a periodic latitude. As such, they can only be compared in this unique geography.

3. Conceptual models

We now proceed to illustrate the wind–buoyancy connection, i.e. we clearly demonstrate that the ocean can always adjust its salinity and temperature field to accommodate the sinking imposed by the wind. To show this, we employ three conceptual analytical models involving the gigantic island. The first two are mixed dynamical-box models of temperature and salinity, respectively. By ‘mixed dynamical-box model’, we mean that the thermodynamic properties of the boxes are completely mixed (i.e. S and T are uniform within each box), but the transports between the boxes are determined dynamically. The third model is a temperature slab model of the upper ocean. Note that our models are fundamentally different from the no-island model of Stommel (1961) and the numerous studies that it initiated, because in his model the interbox transports were dependent only on S and T . In our model, the transports are dependent on the wind alone due to the presence of the island.

3.1. Salinity box model

The salt dynamical-box model consists of an ocean split into two boxes, one south of the southern tip of an island and one north of it (Fig. 5a). To simplify the problem, we now take the northern tip of the island to lie at the North Pole so that a third box north of the island is redundant. (Note that, even though the land mass now extends to the North Pole, it remains an island.) The boxes are a conceptual analog for the oceans south and north of 55°S (the northern latitude of Drake Passage). A net surface flow, Q , from the southern box to the northern box is determined by the wind and the Belt Constraint.

We assume adequate bottom topography at this latitude to enable the return geostrophic flow at depth. On the basis of the observed freshwater fluxes in the ocean, the net surface freshwater flux, F_F , is taken to be positive for the southern box and equal but negative in the northern box (Wijffels et al., 1992). Conservation of salt for the southern box gives

$$\frac{\partial(V_1 S_1)}{\partial t} = (Q - F_F)S_2 - QS_1, \quad (9)$$

where V is the volume of the box, t is the time, S is the salinity and the subscripts 1 and 2 refer to the southern and northern boxes, respectively. We see that an increase in Q acts to make the SO more salty and, similarly, the Northern Ocean becomes fresher. The salinity adjustment continues until a new steady state it reached, namely,

$$S_1 = \left(1 - \frac{F_F}{Q}\right) S_2. \quad (10)$$

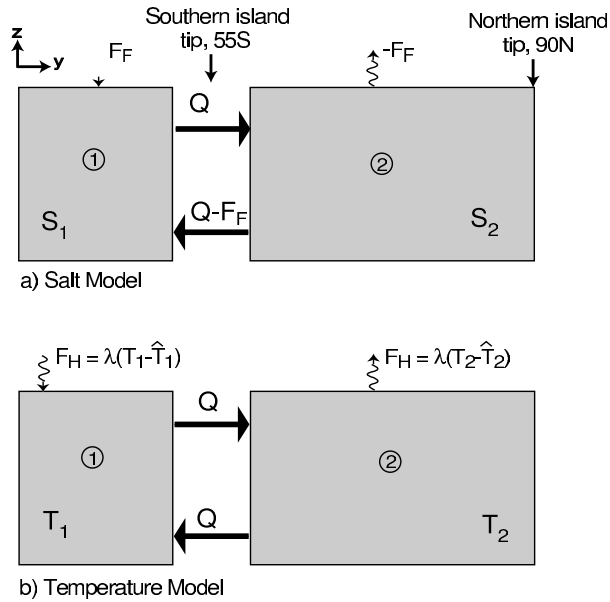


Fig 5. Two box models of (a) salinity (S) and (b) temperature (T). The southern and northern boxes (1 and 2, respectively) are divided at the southern tip of an island (e.g. the Americas) that lies in a latitude belt free of continents. For simplicity, the island is taken to extend to the North Pole, so that an additional third northern box is redundant. The surface transport between the boxes, Q , is determined by the Belt Constraint (eq. 3) and the zonal wind stress at the division. A return flow at depth closes the mass budget. The salinity boxes exchange freshwater, F_F , with the atmosphere. F_F is positive into the southern box and equal but negative into the northern box (Wijffels et al., 1992). The temperature boxes exchange heat, F_H , with the atmosphere in an amount proportional to the difference between T and the atmospheric temperature, \hat{T} . For clarity, the salinity and temperature models are shown separately, but the processes (T and S adjustments) are mutually independent and could have been presented simultaneously.

As the wind-driven transport increases, the salinity difference between the two boxes will merely decrease to accommodate the additional transport. In other words, a constant freshwater flux can convert more lower layer water to upper layer water when the salinity difference between the layers is reduced. In the real ocean, a weaker stratification would produce the same effect. Conversely, weaker Southern winds would intensify the stratification.

3.2. Temperature box model

The temperature field reacts somewhat differently to the winds. Not only does the stratification influence the ease of vertical exchange (as in the salinity case), but it also affects the heat exchange with the atmosphere. Again, we consider a simple box model of the ocean temperature (Fig. 5b). The heat flux, F_H , is taken to be proportional to the difference between the oceanic temperature, T and atmospheric temperature, \hat{T} , so that

$F_H = \lambda(\hat{T} - T)$, where λ is a proportionality constant. This type of parametrization can be regarded as a bulk parametrization of latent and sensible heat loss, or simply as a restoring boundary condition on the upper layer temperature, T (Haney, 1971; Rahmstorf and Willebrand, 1995). For the southern box, the conservation of heat gives

$$\frac{\partial T_1}{\partial t} = \frac{Q}{V_1}(T_2 - T_1) - \frac{\lambda}{C_p \rho H}(T_1 - \hat{T}_1), \quad (11)$$

where C_p is the heat capacity of sea water, V_1 is the box volume, H is the layer depth and ρ is the average water density. The equation for the northern box is similar. For a steady-state ocean (and atmosphere), the total heat flux (i.e. the sum of the heat fluxes into the two boxes) must be zero:

$$\lambda V_1(T_1 - \hat{T}_1) + \lambda V_2(T_2 - \hat{T}_2) = 0. \quad (12)$$

We can now solve analytically for T_1 and T_2 from eqs. (11) and (12)

$$T_{1,2} = \left[\left(\frac{\lambda V_{1,2}}{C_p \rho H Q} + \frac{V_{1,2}}{V_{2,1}} \right) \hat{T}_{1,2} + \hat{T}_{2,1} \right] \times \left[1 + \frac{\lambda V_{1,2}}{C_p \rho H Q} + \frac{V_{1,2}}{V_{2,1}} \right]^{-1}, \quad (13)$$

which, for $\hat{T}_1 = 5^\circ\text{C}$ and $\hat{T}_2 = 15^\circ\text{C}$, is plotted as a function of Q in Fig. 6. For simplicity, the southern box was chosen to be a fifth

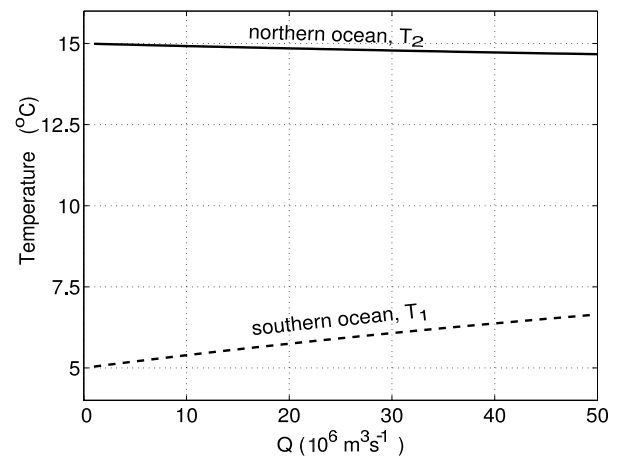


Fig 6. The temperature of the oceanic box model as a function of the transport (Q) between the boxes (13). The solid line shows the temperature of the northern box and the dashed line that of the southern box. Atmospheric temperatures were taken to be $\hat{T}_1 = 5^\circ\text{C}$ and $\hat{T}_2 = 15^\circ\text{C}$. As the transport increases, the oceanic temperature diverts from that of the overlying atmosphere and the temperature difference between the boxes decreases. Therefore, as in the salinity model, the stratification weakens as the winds are increased. The SO is more strongly affected by the transport than the northern ocean because we took its volume to be five times smaller. The parameters are $V_1 = 10^{16} \text{ m}^3$, $V_2 = 5.10^{16} \text{ m}^3$, $\lambda = 50 \text{ W m}^{-2} \text{ K}^{-1}$, $\rho = 1000 \text{ Kg m}^{-3}$, $C_p = 4000 \text{ J Kg}^{-1} \text{ K}^{-1}$, $H = 500 \text{ m}$.

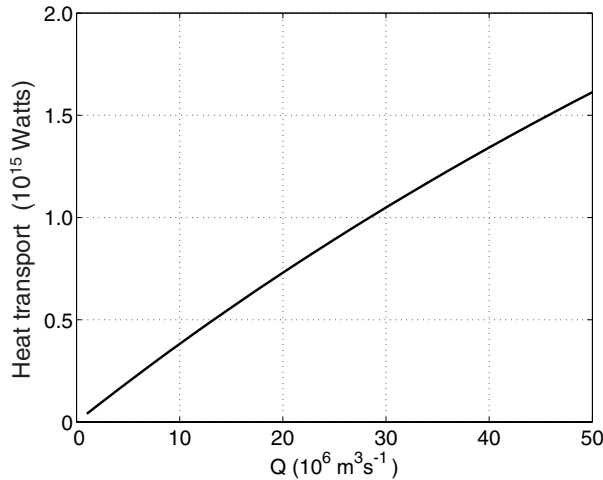


Fig 7. The southward heat transport in the box model as a function of the mass transport (Q) between the boxes (13).

of the northern box. As the transport increases, the oceanic temperature diverts from the atmospheric temperature. The smaller volume of the southern box renders it more vulnerable to the interbox transport. Similar to the salinity box model, the difference in the temperature between the two boxes shrinks in response to stronger southern winds. This is again analogous to a weakening of the oceanic stratification. The heat transport between the boxes is shown in Fig. 7. It increases almost linearly with the wind driven overturning.

A curious situation arises from our choice of atmospheric temperatures and transport direction. The surface flow from the southern box to the northern box is colder than the opposing deep flow, clearly an unstable stratification in a constant salinity ocean. In a more realistic model where the temperature and salinity both vary simultaneously, we expect that salinity will have a stabilizing effect, as the surface water in the south is fresher than the deep water (i.e. $S_1 < S_2$). This unstable flow pattern is a consequence of using a well-mixed box model. The averaging of the box temperatures over a wide latitudinal range introduces unrealistic local temperatures. In other words, even if the deep water that sinks in the NA is near freezing, the overall mean temperature of the upper layer ocean north of 55°S is much higher. This effect is eliminated in a y -dependent slab model of the upper ocean, which is discussed in the next subsection. Also, in the real SA the cold northward flow (compensated by an even colder southward deep flow) causes a net northward heat transport while our heat transport is southward.

3.3. Temperature slab model

Consider a slab of ocean (Fig. 8) whose temperature has explicit y (latitude) dependence. A steady flow (independent of x) passes through the slab at a velocity and flux determined by the wind. The water sinks in the Northern Hemisphere north of

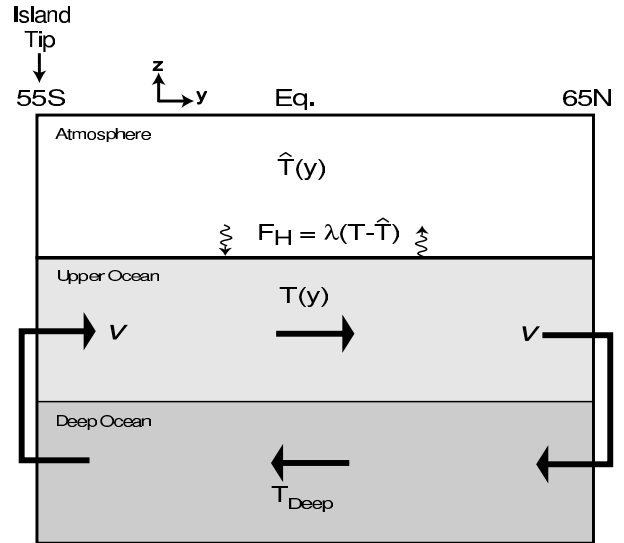


Fig 8. Slab model of the ocean and atmosphere from 55°S to 65°N . The upper layer presents the atmosphere which has a fixed y -dependent temperature profile, $\hat{T}(y)$, depicted in Fig. 9. Below the atmosphere lies the upper ocean which exchanges heat with the atmosphere in an amount proportional to $(T - \hat{T}(y))$. A constant flow of water flows northward in this layer at a constant velocity, v , determined by the Belt Constraint (3) and the zonal wind stress at 55°S . North of 65°N the water is subducted to the deep layer, returns south, and is upwelled again south of 55°S .

65°N , flows southward in the deep ocean and is upwelled south of 55°S . The southern boundary was chosen at the tip of South America and the northern boundary at the average latitude of NA deep convection. The heat exchanges with the atmosphere is $F_H = -\lambda(T - \hat{T})$ while the deep ocean water conserves its temperature. We assume an atmospheric cosine temperature distribution of $\hat{T} = \hat{T}_m + \hat{T}_0 \cos(2y/b)$, where b is the radius of the Earth, \hat{T}_m is the average temperature and \hat{T}_0 is the amplitude of the variation around the mean (Fig. 9). Conservation of heat yields

$$\frac{\partial T}{\partial t} = -v \frac{\partial T}{\partial y} - \frac{\lambda}{C_p \rho H} (T - \hat{T}), \tag{14}$$

where v is the fixed meridional velocity of the flow through the slab (given by the wind). The analytical solution of eq. (14) is

$$T = \hat{T}_m + \frac{a^2 \hat{T}_0}{a^2 + d^2 v^2} \cos dy + \frac{ad \hat{T}_0 v}{a^2 + d^2 v^2} \sin dy + Ae^{-(ay/v)}, \tag{15}$$

where $a = \lambda / (C_p \rho H)$, $d = 2/b$, and A is an integration constant to be determined. We solve for A by recognizing that, to conserve heat in the ocean, the incoming and outgoing temperatures must be equal. The final analytical solution is straightforward and is depicted in Fig. 9 for two different velocities: $v = 1 \text{ cm s}^{-1}$ and $v = 10 \text{ cm s}^{-1}$.

Without any meridional transport, the ocean adopts the temperature profile of the atmosphere as its own temperature field. As

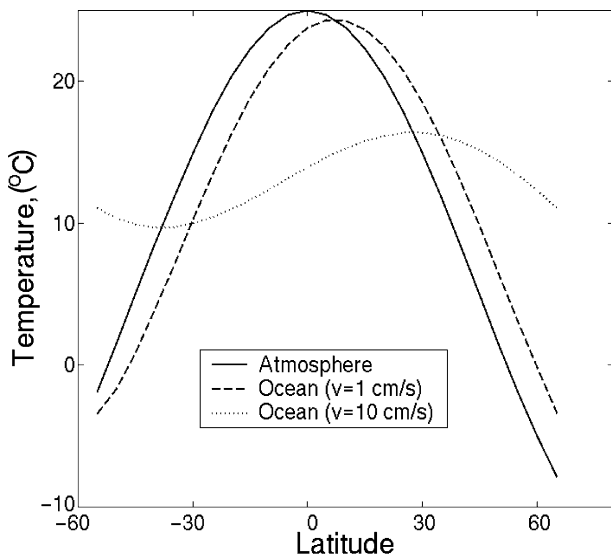


Fig 9. Analytical atmospheric and oceanic temperature profiles of the slab model. The solid line shows the fixed atmospheric cosine function. The dashed and dotted lines are the solutions of eq. (14) for the two velocities, $v = 1 \text{ cm s}^{-1}$ and $v = 10 \text{ cm s}^{-1}$. The other parameter choices were $T_m = 278 \text{ K}$, $T_0 = 20 \text{ K}$, $\lambda = 50 \text{ W m}^{-2} \text{ K}^{-1}$, $\rho = 1000 \text{ K gm}^{-3}$, $C_p = 4000 \text{ J Kg}^{-1} \text{ K}^{-1}$, $H = 1000 \text{ m}$. Increasing velocities flatten the oceanic temperature profile and shift its peaks northward.

the velocity (and, hence, the transport) is increased, the oceanic solution shifts northward, away from the atmospheric temperature profile. The north-south asymmetry produces a net northward heat transport across the equator. In addition to the shift between the temperature peaks of the ocean and atmosphere, stronger velocities tend to flatten the oceanic temperature profile. This is again akin to a weaker stratification. It should be noted that, in reality, the atmospheric profile is also dependent on the oceanic temperatures. This would add another feedback which is presently neglected.

4. Numerical simulations

In this section we confirm our earlier analytical results numerically (i.e. using process-oriented numerical simulations, we show that the ocean will adjust itself to allow the overturning forced by the SO winds). The model we use is a simple reduced gravity model that has been derived from the isopycnal model originally developed by Bleck and Boudra (1981, 1986). We include two different thermodynamic parametrization (details described below) and then for each we perform six runs of increasing southern wind stress to test the overturning's response.

4.1. Model description

The process-oriented model is a layer-and-a-half model, which means that the lower layer is assumed to be infinitely deep and

at rest. A dynamic upper layer is governed by the continuity equation and the non-linear frictional momentum equations

$$\begin{aligned} \frac{\partial u}{\partial t} + u \frac{\partial u}{\partial x} + v \frac{\partial u}{\partial y} - \widehat{\beta} y v \\ = -g' \frac{\partial h}{\partial x} + \frac{v}{h} \nabla \cdot (h \nabla u) + \frac{\tau^x}{\rho h} - K u, \end{aligned} \quad (16)$$

$$\begin{aligned} \frac{\partial v}{\partial t} + u \frac{\partial v}{\partial x} + v \frac{\partial v}{\partial y} + \widehat{\beta} y u \\ = -g' \frac{\partial h}{\partial y} + \frac{v}{h} \nabla \cdot (h \nabla v) + \frac{\tau^y}{\rho h} - K v, \end{aligned} \quad (17)$$

where u and v are the zonal and meridional velocities, $\widehat{\beta}$ is the derivative of the Coriolis parameter with respect to y , g' is the reduced gravity, h is the upper layer thickness, ν is the viscosity, K is the linear drag coefficient and τ^x and τ^y are the zonal and meridional wind stresses, respectively. The equations are solved using an Arakawa C-grid (Arakawa, 1966) finite difference expansion and the leap-frog scheme to advance in time.

Following Nof (2000, 2002, 2003), we made our runs more economical by reducing the grid points in the x and y directions by 15, and increasing the wind stress and β correspondingly. More specifically, Δx and Δy in our model are both 15 km and we have 68 grid points in the y direction and 42 in the x direction. However, by increasing both τ and β by 15, the basin represents a domain extending from 68°S to 68°N and covering 9450 km in the zonal direction. A thin meridional island lies between 53°S and 65°N (Fig. 10a).

These grid modifications lead to a reduction in the grid count (and consequently, the run time) by a factor of 15^2 . The downside of the above modifications is an unnaturally large ratio between the eddy size and the basin size. This is not a problem in our runs

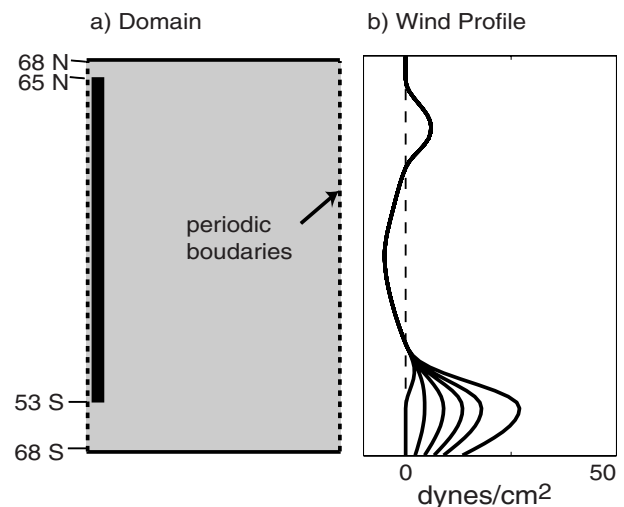


Fig 10. Description of the numerical model. The basin extends from 68°S to 68°N and is periodic in the zonal direction. An elongated island lies on the left between 53°S and 65°N . Winds are adapted from Hellerman and Rosenstein (1983) (b). South of the island, the winds are successively increased by a factor ranging from 0 to 3.

Table 1. The 12 experiments. Common model parameters are $\Delta x = 15$ km, $\Delta y = 15$ km, $\Delta t = 360$ s, $g\tau = 0.015$ ms⁻², $H = 800$ m, $\hat{\beta} = 3.4 \times 10^{-10}$ m⁻¹ s⁻¹, $\nu = 1600$ m² s⁻², $K = 2 \times 10^{-6}$ s⁻¹, $\hat{h}_m = 800$ m, $\hat{h}_0 = 100$ m

	Experiment number	Wind amplitude
Set A	1	0
$W_{F0} = 2 \times 10^{-4}$ m s ⁻¹	2	0.1
$c_1 = 2 \times 10^{-6}$ s ⁻¹ , $c_2 = 0$	3	1
	4	1.5
	5	2
	6	3
Set B	7	0
$W_{F0} = 0$, $c_1 = 3 \times 10^{-6}$ s ⁻¹	8	0.1
$c_2 = 1.5 \times 10^{-7}$ cm ⁻¹	9	1
	10	1.5
	11	2
	12	3

because the eddies do not play a major role in the meridional mass exchange. Furthermore, this unnatural eddy–basin ratio issue can be easily resolved by using a very large horizontal eddy viscosity coefficient that eliminates any long-lived eddies such as Gulf Stream rings. This essentially implies that our model is not an eddy-resolving model. Note also that, with our chosen parameters, the ratio between the Munk layer thickness $(\nu/\hat{\beta})^3$ and the basin size was still very small (as required) because our $\hat{\beta}$ was magnified.

Winds are adapted from the zonally averaged Hellerman and Rosenstein (1983) data set. For each of the two thermodynamic parametrizations, the wind stress south of the island is magnified by factors ranging from 0 to 3 (Fig. 10b). The resulting 12 runs are summarized in Table 1.

4.2. Thermodynamic forcing

Two sets of experiments (A and B) were run, which differ in their thermodynamic parametrizations (Fig. 11). In set A, we represent both heat and saltwater fluxes and use a uniform mixing coefficient. For the second set, B, we consider only a heat flux approximation but, here, we increase the mixing in polar regions (relative to the equator) to mimic observations of more convection in high latitudes. Both approaches are described in more detail below.

Recall that, in a reduced gravity model the density of the upper layer is constant, so that buoyancy fluxes that would induce a density increase (decrease) in the upper layer can only be represented by a decrease (increase) of the upper layer thickness. This translates to a vertical velocity, w , in the continuity equation

$$\frac{\partial h}{\partial t} + \frac{\partial(hu)}{\partial x} + \frac{\partial(hv)}{\partial y} = w = w_F + w_H, \quad (18)$$

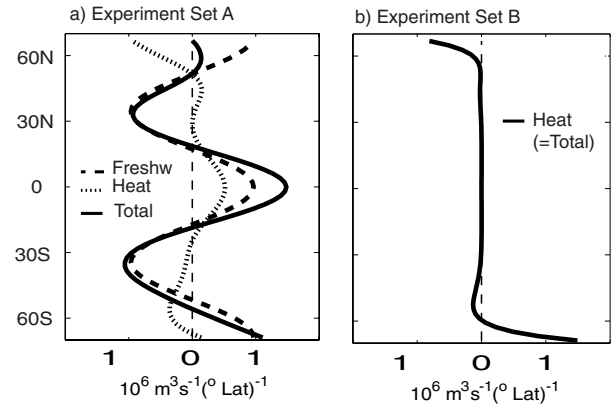


Fig. 11. Buoyancy forcing for sets A and B. An imposed buoyancy flux at the surface is converted to a source or sink of upper layer water. For set A, the freshwater flux (dashed line) is a fixed profile, while the heat flux (dotted line) depends on the upper layer thickness (see text for more details). The buoyancy south of 55°S is provided by the freshwater flux which allows a negative heat buoyancy flux. For set B, the freshwater flux is neglected and the heat fluxes at the poles are exaggerated compared to the equator. In the absence of freshwater flux, which provides buoyancy to the SO, the heat flux itself must provide the required buoyancy. Both heat flux profiles are for a wind amplification factor of 1 (experiments 3 and 9). Note that, for stronger winds, the heat buoyancy flux in the SO is positive also for the experiments in set A because the freshwater flux is then inadequate for providing the required buoyancy.

where w_F is the contribution from the freshwater flux and w_H from the heat flux. The parametrization of w_F is straightforward. We assume a zonally independent distribution that varies in latitude according to a cosine function

$$w_F = w_{F0} \cos \frac{2\pi j}{68}, \quad (19)$$

where w_{F0} is the amplitude of the function (shown in Fig. 11a) and j is the latitude. Positive peaks, representing high precipitation regions, are at the equator and the poleward boundaries; evaporative regions peak at the subtropics. All parameter choices are given in the caption of Table 1. For set B, $w_{F0} = 0$.

Our heat flux parametrization is similar to that used by Cushman-Roisin (1987) in a two-layer analytical model and by Spall (2002) in a numerical reduced gravity model (see also Kawase, 1987). The heat buoyancy flux w_H is assumed to be proportional to the difference between the oceanic and atmospheric temperatures. As mentioned earlier, this type of parametrization can be regarded as a bulk parametrization of latent and sensible heat loss, or simply as a restoring boundary condition on the upper layer temperature, T (Rahmstorf and Willebrand, 1995). In the absence of an explicit temperature variable, the upper layer thickness, h , is used as a proxy for T . The motivation for this choice lies in the fact that in a reduced gravity model (which, by definition, has a constant upper layer density) Δh is proportional

to ΔT . The atmospheric temperature, \hat{T} , is likewise converted to length dimensions, \hat{h} , so that the vertical velocity is

$$w_H = -\alpha(h - \hat{h}), \quad (20)$$

where α is a proportionality constant which is constant in set A. In this simple system, the heat gain or loss by the atmosphere is directly conveyed to the deep layer at the position and time of input. For example, to conserve the upper layer density, a cooling event in the NA would immediately result in sinking of water to the lower layer. This is, of course, a rather coarse approximation, especially in low latitude where water mass conversion is limited. Consequently, the sources of upper layer water in the tropics and subtropics are exaggerated. In set B, we simulate more mixing/convection in high latitudes by letting α decline exponentially from the poles to the equator so that

$$\alpha = c_1 e^{-c_2 |y_b - y|}, \quad (21)$$

where c_1 and c_2 are constants given in Table 1, and $|y_b - y|$ is the distance away from the the northern and southern boundaries.

Our parametrization differs from that of Cushman-Roisin (1987) and Spall (2002) in that they assumed a constant \hat{h} , whereas we take \hat{h} as a cosine function of latitude

$$\hat{h} = \hat{h}_m + \hat{h}_0 \cos \frac{2\pi j}{136}, \quad (22)$$

where \hat{h}_m is the mean and \hat{h}_0 is the amplitude of the function. The atmospheric ‘temperature’ peaks at the equator and decreases towards the poles. However, the heat flux distribution does not resemble the atmospheric temperature profile closely because it also depends on the thickness (temperature) of the upper layer. Figure 11 depicts the profile of the heat flux for the run in each set where the wind amplification factor was one. The buoyancy flux due to heating in the SO is negative for set A. Hence, the required buoyancy gain is provided by the freshwater. In the absence of freshwater forcing (set B) all the buoyancy is provided by the heat flux so that the heat buoyancy flux is positive (corresponding to a very thin upper layer in the SO).

4.3. Results

As mentioned, 12 runs (two sets, A and B, for which the southern wind stress was amplified by a factor of 0–3) were executed. The upper layer thickness for the control run (wind amplification factor 1) is shown in Fig. 12. For each run, the integrated transport across the 55°S latitude was computed. In Fig. 13 the results for set A are compared to the theoretical transport given by the Belt Constraint (3). We see that the flow across the open latitude band follows very closely the increase in the wind stress at that latitude. The difference is due to lateral friction, linear drag and advection in the model (Fig. 14). Even though a circumpolar current forms in the south, the friction associated with the current at the island tip is negligible. A similar correlation between the wind and transport across 55° is found for set B (Fig. 15).

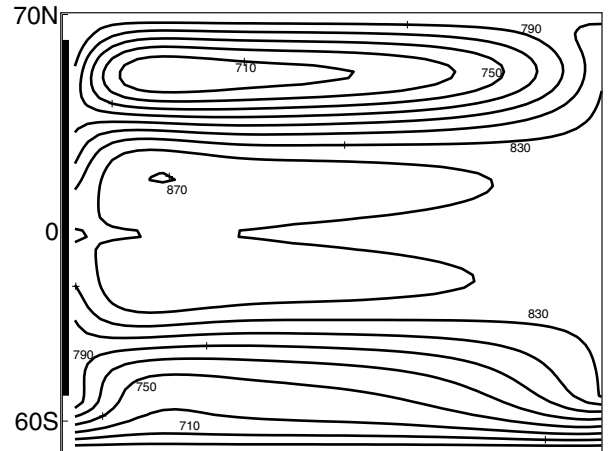


Fig 12. Contours of upper layer thickness (in meters) for set A, experiment 3. The wind amplification factor is 1.

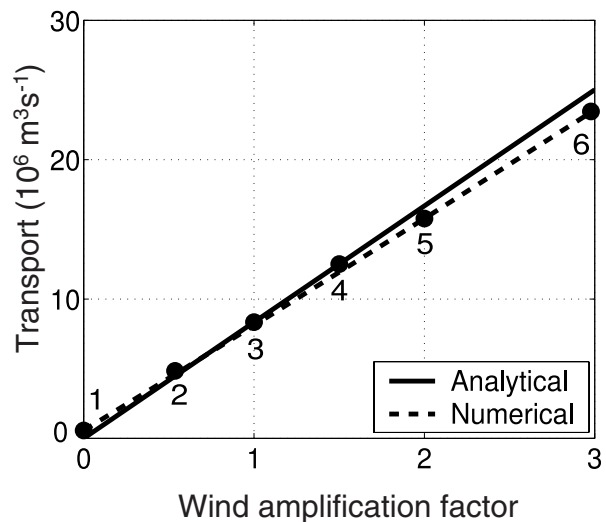


Fig 13. Transport across 55°S , the latitude just south of the island (Fig. 9) for experiments in set A. The solid line is the analytical transport determined by the Belt Constraint (3). The dashed line shows the dependence of the numerical transport on the increased winds. Each bullet indicates a different run and is labeled by its experiment number (Table 1). The numerical flow agrees very closely with the Belt Constraint. The minute differences are due to lateral friction, linear drag and advection in the numerical model as indicated in Fig. 14.

The model adapts to stronger winds by decreasing its upper layer thickness (equivalent to cooling) in the south and increasing it northward of 55°S (Fig. 16). As a result, heat loss to the atmosphere in the SO is reduced, the net buoyancy flux (freshwater plus heat) becomes more positive and, hence, more deep water is upwelled. Northward of 55°S , the deeper upper layer (or thermocline) loses more heat to the atmosphere so that sinking is enhanced. This response was also found by Bjornsson and Toggweiler (2001) in a multilayered ocean model coupled to a

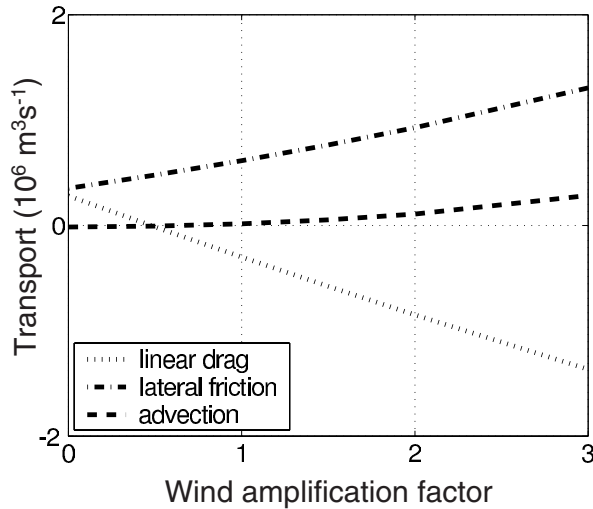


Fig 14. Numerical terms of experiments in set A which were neglected in the analytical derivation of the Belt Constraint transport. To compare the terms with the Belt Constraint results, units were converted to volume flux through a division by the Coriolis parameter at 55°S. Together, the linear drag (dotted line), lateral friction (dash-dotted line) and advection (dashed line) account for the difference between the analytical and numerical solutions in Fig. 13.

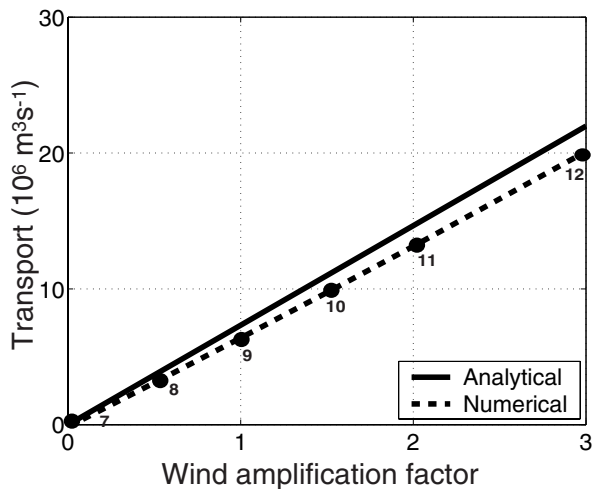


Fig 15. Transport across 55°S for experiments in set B. As in Fig. 13, the solid line is the analytical transport determined by the Belt Constraint (3), while the dashed line shows the dependence of the numerical transport on the increased winds. Each bullet is labeled by its experiment number (Table 1). Here, too, the numerical flow agrees very closely with the Belt Constraint.

atmospheric energy balance model. Conversely, weaker winds result in a warmer SO and cooler northern ocean.

4.4. Weaknesses

Before continuing, it is appropriate to discuss the main weaknesses of the model, as follows.

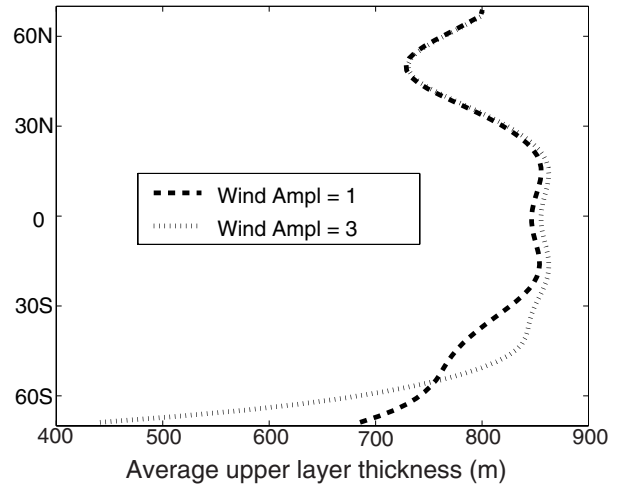


Fig 16. Zonally averaged upper layer thickness for experiments 3 (wind amplification factor of 1) and 6 (wind amplification factor of 3). The response to stronger winds occurs mainly in the Southern Hemisphere. In the case of stronger SO winds, the upper layer in the south becomes thin so that the ocean takes up heat from the atmosphere. For standard winds, the upper layer in the south is thicker (warmer) than the atmospheric thickness and, therefore, it loses heat to the atmosphere. In this case buoyancy is provided by the freshwater flux (see Fig. 11).

(i) The use of the upper layer thickness as a proxy for the temperature is obviously potentially problematic. It is motivated by the following logic. For the density of the layer to remain constant while it is receiving heat from the atmosphere, h will have to increase in lieu of T . In other words, the heat is used to transform lower layer water to upper layer water instantly. However, in the real ocean, the heat from the atmosphere is not necessarily used locally for water mass conversion and, in that sense, our model misrepresents the ocean.

(ii) The heat flux is assumed to be proportional to the upper layer thickness (used as a proxy for the temperature). This is also potentially problematic because processes such as the freshwater flux and divergence of the flow field also affect h . These processes are therefore artificial components of our heat flux.

(iii) The conversion of the atmospheric temperature profile to ocean thickness units cannot be done rigorously. The choices of the atmospheric depth profile and heat flux proportionality constant were therefore somewhat arbitrary. We chose α roughly so that an average $(h - \hat{h})$ of 100 m in the SO would produce a source of 15 Sv. Doubling or halving of this value changes our results (which is the transport across 55°S) by less than 10%.

(iv) The freshwater flux parameter, $w_{F0} = 2 \times 10^{-4} \text{ m s}^{-1}$, was chosen in a similar fashion. It results in a source of 7 Sv in the SO. As in the case of the heat flux parameter, doubling or halving of w_{F0} changes our results by less than 10%.

(v) There is no feedback between the oceanic and the atmospheric temperatures. In reality, the temperature of the atmosphere is not fixed, but rather tends to follow the oceanic profile.

Overall, our buoyancy flux parametrization is not ideal. Yet it offers a compromise between a more complicated multilayered ocean general circulation model and a simple reduced gravity model without any thermodynamics. The former is computationally expensive to use as a process-oriented tool and, more importantly, is very difficult to interpret, while the latter is for obvious reasons not adequate for our analysis. Our middle of the way choice seem to be the best tool to use.

5. Discussion

In the last decade several studies have found a link between the global overturning circulation and the SO winds. The controversial implication of such a link is that the seemingly independent wind and buoyancy forcings must be coupled. We derived here the wind–thermodynamic connection formally in the framework of a single meridional island (on a sphere) that lies between latitudinal bands free of continents. The presence of such an island enables us to treat the problem analytically.

At the island tips, the meridional transport is given by the Belt Constraint (3), which is a zonally integrated version of the linearized x -momentum equation. In essence, the Belt Constraint requires that the northward transport above the topography be equal to the Ekman transport because the net geostrophic transport is zero. Eddy fluxes in the latitudinal corridor between the SA and the Antarctic circumpolar current were neglected in the analysis, as it is not clear how large their contribution is, how they will respond to the wind and how to include them. The difference between the Belt Constraints at the two island tips yields the amount of water that needs to sink (or rise) through the upper layer adjacent to the island. We have derived a thermodynamic version of Godfrey's IR by including the sinking (or rising) in the basin east of the island (eqs. 7 and 8) and we have shown that it is consistent with the Belt Constraint (3).

We have illustrated the alignment of buoyancy to wind forcing qualitatively, using two gigantic island dynamical-box models (Fig. 5) and an island slab model (Fig. 8), and semiquantitatively with the aid of a numerical reduced gravity model (Fig. 10). The three conceptual models all carry a northward surface transport that is forced by the wind field and the Belt Constraint. The adjustment of the salinity field in the first box model to stronger southern winds is readily understood. Following an increase in the wind stress, additional conversion of water between the boxes is brought about by a reduction in the salinity difference between the boxes. In reality, vertical isohalines (such as the division between the boxes) do not exist. Rather, the boxes should be regarded partly as southern and northern boxes, and partly as upper layer and deep ocean boxes. The reduction in the salinity difference is therefore analogous to a weakening of both the horizontal and vertical stratification in the real ocean.

Likewise, the temperature field of the box model adjusts to the wind field, although the reaction is complicated by the feedback of the temperature on the surface heat flux. An increase in south-

ern winds tends to reduce the temperature difference between the boxes so that, again, the stratification is weakened (Fig. 6). An island slab ocean model (which is y -dependent) was used to give a richer picture of the influence of the wind on the meridional temperature distribution. It was found that, for very weak winds (small meridional transport), the ocean temperature equilibrates with the atmosphere. Stronger winds have two effects. First, they shift the temperature profile northward (so that it lags the atmospheric profile) and, secondly, the amplitude of the variations around the mean is reduced (Fig. 9). This is akin to a weaker stratification in the real ocean.

The island wind–buoyancy link was next explored semiquantitatively using a reduced gravity numerical model. Buoyancy forcing was included by adding a mass flux term in the continuity equation. The term consists of a variable heat flux contribution and a freshwater flux contribution that is fixed in time but has y dependence. The heat flux is proportional to the difference between the upper layer temperature (approximated by the upper layer thickness) and an atmospheric temperature (converted to thickness units). Two different choices for the heat and freshwater contribution were assumed. The numerical model domain is a periodic ocean that contains only one long meridional island. A series of runs was performed where the southern winds were increased by a factor ranging from 0 to 3. The transport across the latitude of the southern island tip (Fig. 10a) was calculated for each buoyancy parametrization and an excellent agreement was found with the Belt Constraint (3). As the winds increased, the thermocline in the north deepened ('warmed') and shallowed ('cooled') in the south. In our model, the additional sinking from increased winds occurs mostly in the SA (Fig. 16). More sophisticated numerical models suggest that additional sinking due to increased winds occurs partly in the SA through a more vigorous (isopycnic) Deacon cell and partly in the NA via enhanced NADW formation. Our SA buoyancy driven sinking seems to be a mix of these two processes. Note also that the numerical model, having only one layer and a fixed reduced density, lacks the ability to resolve the effect of weaker stratification on the sinking (seen in the box models). Instead, it makes use of the feedback of the ocean temperature on the surface heat flux to accommodate the required sinking.

6. Conclusions

We have considered a one-on-one relationship between the SO winds and the MOC for a gigantic island on a sphere. This unique geometry leads to simple analytical solutions. We have neglected the effect of SO eddy fluxes and assumed that all the sinking north of Drake Passage occurs in the NA. In numerical models, a significant part of the northward transport sinks and returns southward in the Southern Hemisphere Deacon cell through isopycnal flows. In theory, all the northward flowing water could return through this pathway, especially because we have not assumed a level of no motion, but merely integrated

to a fixed depth above the topography (so that vertical isopycnal transport is possible). Nevertheless, numerical models show a response of NADW outflow to an increase in SO winds and it is this mechanism which we are interested in. This idealized setup was therefore constructed to isolate the thermodynamical link between the SO winds and Northern Hemisphere sinking. More specifically, we addressed the question of how, in a steady-state ocean, a given buoyancy forcing distribution can overturn transports prescribed by the SO winds.

In view of our theoretical and numerical results, we conclude that the coupling between the wind and the surface buoyancy forcing occurs through an adjustment in the ocean stratification. As a response to stronger winds, both the temperature and salinity fields become more weakly stratified in our model and, in addition, the thermocline deepens in the north. A weaker stratification after an increase of SO winds was also found (although not explicitly pointed out) in the numerical model of Bjornsson and Toggweiler (2001).

At first glance this result may seem simple, but it is quite subtle. We are tempted to conclude that the wind thus provides the energy to set up the density distribution in such a way that it will force an overturning in the ‘traditional sense’ of a thermohaline driven circulation. By ‘traditional sense’ we mean here the common practice of parametrizing the overturning to be proportional to the density differences between the boxes (see, for example, Stommel, 1961; Park, 1999; Marotzke, 2000, and references therein). By contrast, our box model results suggest that it is the overturning circulation that controls the density differences, and not vice versa. Note, however, that all simple box models of the overturning (with or without an island) suffer from the fact that they cannot resolve fine-scale spatial processes. Consequently, it is assumed that the density of the water that is exchanged between the boxes is equal to the average box density. Therefore, it is dangerous to draw conclusions from them with regard to the detailed large-scale stratification. Our results should be used as a warning against the overuse of density differences as a proxy for interbox transports in future MOC models.

7. Acknowledgments

This study was supported by the National Aeronautics and Space Administration under grants NAG5-7630 and NGT5-30164, the National Science Foundation contract OCE 9911324, and the Office of Naval Research grant N00014-01-0291.

8. Appendix: Nomenclature

a	constant, $a = \lambda / (C_p \rho_0 H)$
A	integration constant for slab model
b	radius of the Earth
$c_{1,2}$	constants used in defining α
C_p	heat capacity of sea water

d	constant, $d = 2/b$
f	Coriolis parameter
$f_{1,2}$	Coriolis parameters along the southern and northern island tips (Fig. 4)
g'	reduced gravity
h	upper layer thickness in numerical model
\hat{h}	proxy for atmospheric temperature in depth units
\hat{h}_m	mean of \hat{h}
\hat{h}_0	amplitude of the variation in \hat{h}
H	depth of box and slab model
j	latitude
K	linear drag coefficient
P	vertically integrated pressure
Q	transport between southern and northern boxes (Fig. 5)
$Q_{1,2}$	transports across the latitudes of the southern and northern island tips (Fig. 2)
r	integration path
R	interfacial friction coefficient
$S_{1,2}$	salinities in the southern and northern boxes (Fig. 5)
T	temperature of slab model (Fig. 8)
\hat{T}	atmospheric temperature in slab model (Fig. 8)
\hat{T}_m	mean atmospheric temperature in slab model (Fig. 8)
\hat{h}_0	variation of atmospheric temperature in slab model (Fig. 8)
$T_{1,2}$	temperatures in the southern and northern boxes (Fig. 5)
u, v, w	velocities in the $x, y,$ and z directions
U, V	vertically integrated transports in the x and y direction
$V_{1,2}$	volumes of the southern and northern boxes (Fig. 5)
$w_{F,H}$	vertical velocities associated with freshwater and heat fluxes
w_{F0}	amplitude of variation in w_F
W	net sink of water adjacent to the island
α	proportionality constant for heat flux, $w_H = -\alpha(h - \hat{h})$
$\hat{\beta}$	variation of the Coriolis parameter with y
λ	proportionality constant for surface heat flux
ν	viscosity
ρ_0	average density
τ^r	wind stress along the integration path r
$\tau^{x,y}$	wind stress in the x and y directions
IR	Island Rule
MOC	meridional overturning circulation
NA	North Atlantic
NADW	North Atlantic Deep Water
SO	South Ocean

References

- Arakawa, A. 1966. Computational design for long-term numerical integration of the equations of fluid motion. Two-dimensional incompressible flow. Part I. *J. Comput. Phys.* **1**, 119–143.

- Bjornsson, H. and Toggweiler, J. R. 2001. The climatic influence of Drake Passage. In: *The Oceans and Rapid Climate Change: Past, Present, and Future* (eds D. Seidov, B. J. Haupt, and M. Maslin). Geophysical Monograph Vol. 126, American Geophysical Union, 243–259.
- Bleck, R. and Boudra, D. 1981. Initial testing of a numerical ocean circulation model using a hybrid, quasi-isopycnic vertical coordinate. *J. Phys. Oceanogr.* **11**, 755–770.
- Bleck, R. and Boudra, D. 1986. Wind-driven spin-up in eddy-resolving ocean models formulated in isopycnic and isobaric coordinates. *J. Geophys. Res.* **91**, 7611–7621.
- Broecker, W. S. 1987. The biggest chill. *Nat. Hist.* **10**, 74–82.
- Cushman-Roisin, B. 1987. On the role of heat flux in the Gulf Stream–Sargasso Sea subtropical gyre system. *J. Phys. Oceanogr.* **17**, 2189–2202.
- Döös, K. 1994. Semi-analytical simulation of the meridional cells in the Southern Ocean. *J. Phys. Oceanogr.* **24**, 1281–1294.
- Döös, K. and Coward, A. 1997. The Southern Ocean as the major upwelling zone of North Atlantic deep water. *WOCE Newsletter* **27**, 3–17.
- Döös, K. and Webb, D. J. 1994. The Deacon cell and the other meridional cells of the Southern Ocean. *J. Phys. Oceanogr.* **24**, 429–442.
- Firing, E., Qiu, B. and Miao, W. 1999. Time-dependent island rule and its application to the time-varying North Hawaiian ridge current. *J. Phys. Oceanogr.* **29**, 2671–2688.
- Ganachaud, A. and Wunsch, C. 2000. Improved estimates of global ocean circulation, heat transport and mixing from hydrographic data. *Nature* **408**, 453–456.
- Gill, A. E. and Bryan, K. 1971. Effects of geometry on the circulation of a three-dimensional Southern Hemisphere ocean model. *Deep-Sea Res.* **18**, 685–721.
- Gille, S. 1997. The southern ocean momentum balance: evidence for topographic effects from numerical model output and altimetry data. *J. Phys. Oceanogr.* **27**, 2219–2232.
- Gnanadesikan, A. 1999. A simple predictive model for the structure of the oceanic pycnocline. *Science* **6**(14), 2077–2079.
- Godfrey, J. S. 1989. A Sverdrup model of the depth-integrated flow for the ocean allowing for island circulations. *Geophys. Astrophys. Fluid Dyn.* **45**, 89–112.
- Greatbatch, R. J. and Lu, J. 2003. Reconciling the Stommel box model with the Stommel–Arons model: a possible role for Southern Hemisphere wind forcing. *J. Phys. Oceanogr.* **33**(8), 1618–1632.
- Haney, R. L. 1971. Surface thermal boundary condition for ocean circulation models. *J. Phys. Oceanogr.* **1**, 214–248.
- Hellerman, S. and Rosenstein, M. 1983. Normal monthly wind stress over the world ocean with error estimates. *J. Phys. Oceanogr.* **13**, 1093–1104.
- Karsten, R., Jones, H. and Marshall, J. 2002. The role of eddy transfer in setting the stratification and transport of a circumpolar current. *J. Phys. Oceanogr.* **32**, 39–54.
- Kawase, M. 1987. Establishment of deep ocean circulation driven by deep-water production. *J. Phys. Oceanogr.* **17**, 2294–2317.
- Klinger, B. A., Drijfhout, S., Marotzke, J. and Scott, J. R. 2003. Sensitivity of basin-wide meridional overturning to diapycnal diffusion and remote wind forcing in an idealized Atlantic–Southern Ocean geometry. *J. Phys. Oceanogr.* **33**, 249–266.
- Law, C. S., Abraham, E. R., Watson, A. J. and Liddicoat, M. I. 2003. Vertical eddy diffusion and nutrient supply to the surface mixed layer of the Antarctic Circumpolar Current. *J. Geophys. Res.* **108**(C8), doi:10.1029/2002JC001604.
- Ledwell, J. R., Watson, A. J. and Law, C. S. 1993. Evidence for slow mixing across the pycnocline from an open-ocean tracer-release experiment. *Nature* **364**, 701–703.
- Ledwell, J. R., Watson, A. J. and Law, C. S. 1998. Mixing of a tracer in the pycnocline. *J. Geophys. Res.* **103**(C10), 21 499–21 529.
- McDermott, D. A. 1996. The regulation of northern overturning by southern winds. *J. Phys. Oceanogr.* **26**, 1234–1255.
- Marotzke, J. 2000. Abrupt climate change and thermohaline circulation: mechanisms and predictability. *Proc. Nat. Acad. Sci.* **97**, 1347–1350.
- Munk, W. H. 1966. Abyssal recipes. *Deep-Sea Res.* **13**, 707–730.
- Naveira Garabato, A. C., Polzin, K. L., King, B. A., Heywood, K. J. and Visbeck, M. 2004. Widespread intense turbulent mixing in the Southern Ocean. *Science* **303**, 210–213.
- Nof, D. 2000. Does the wind control the import and export of the South Atlantic? *J. Phys. Oceanogr.* **6**(14), 2650–2667.
- Nof, D. 2002. Is there a meridional overturning cell in the Pacific and Indian Oceans? *J. Phys. Oceanogr.* **32**, 1947–1959.
- Nof, D. 2003. The Southern Ocean's grip on the northward meridional flow. *Prog. Oceanogr.* **56**, 223–247.
- Nof, D. and De Boer, A. M. 2004. From the Southern Ocean to the North Atlantic in the Ekman layer? *Bull. Am. Meteorol. Soc.* **85**, 79–87.
- Park, Y.-G. 1999. The stability of thermohaline circulation in a two-box model. *J. Phys. Oceanogr.* **29**, 3101–3110.
- Pedlosky, J., Pratt, L. J., Spall, M. A. and Helfrich, K. R. 1997. Circulation around islands and ridges. *J. Marine Res.* **55**, 1199–1251.
- Polzin, K. L., Toole, J. M. and Schmitt, R. W. 1995. Fine-scale parametrizations of turbulent dissipation. *J. Phys. Oceanogr.* **25**, 306–328.
- Rahmstorf, S. and England, M. H. 1997. Influence of Southern Hemisphere winds on North Atlantic Deep Water flow. *J. Phys. Oceanogr.* **27**, 2040–2054.
- Rahmstorf, S. and Willebrand, J. 1995. The role of temperature feedback in stabilizing the thermohaline circulation. *J. Phys. Oceanogr.* **25**, 787–805.
- Rintoul, S. R., Hughes, C. W. and Olbers, D. 2001. The Antarctic Circumpolar Current System. In: *Ocean Circulation and Climate* (eds G. Siedler, J. Church, and J. Gould). Academic Press, New York, 271–302.
- Sloyan, B. M. and Rintoul, S. R. 2001. The Southern Ocean limb of the global overturning circulation. *J. Phys. Oceanogr.* **31**, 143–173.
- Spall, M. A. 2002. Wind- and buoyancy-forced upper ocean circulation in two-strait marginal seas with application to the Japan/East Sea. *J. Geophys. Res.* **107**(C1), 6.1–6.12.
- Speer, K., Rintoul, S. R. and Sloyan, B. 2000. The diabatic deacon cell. *J. Phys. Oceanogr.* **30**, 3212–3222.
- Stanton, B. R. 2001. Estimating the East Auckland Current transport from model winds and the island rule. *New Zealand J. Marine Freshwater Res.* **35**, 531–540.
- Stevens, D. P. and Ivchenko, V. O. 1997. The zonal momentum balance in an eddy resolving general-circulation model of the Southern Ocean. *Q. J. R. Meteorol. Soc.* **123**, 929–951.

- Stommel, H. 1961. Thermohaline convection with two stable regimes of flow. *Tellus* **2**, 224–230.
- Toggweiler, J. R. and Samuels, B. 1993. Is the magnitude of the deep outflow from the atlantic ocean actually governed by southern hemisphere winds? In: *The Global Carbon Cycle* (eds M. Heinmann). NATO ASI Series, Vol. I 15, Springer-Verlag, Berlin, 303–331.
- Toggweiler, J. R. and Samuels, B. 1995. Effect of Drake Passage in the global thermohaline circulation. *Deep-Sea Res.* **42**, 477–500.
- Toggweiler, J. R. and Samuels, B. 1998. On the ocean's large-scale circulation near the limit of no vertical mixing. *J. Phys. Oceanogr.* **6**(14), 1832–1852.
- Tsujino, H. and Sugimoto, N. 1999. Thermohaline circulation enhanced by wind forcing. *J. Phys. Oceanogr.* **29**, 1506–1516.
- Webb, D. J. and Sugimoto, N. 2001. The interior circulation of the ocean. In: *Ocean Circulation and Climate* (eds G. Siedler, J. Church, and J. Gould). Academic Press, New York, 205–214.
- Wijffels, S. E., Schmitt, R. W., Bryden, H. L. and Stigebrandt, A. 1992. Transport of freshwater by the oceans. *J. Phys. Oceanogr.* **22**, 155–162.
- Wunsch, C. 2002. What is the thermohaline circulation? *Science* **298**(5596), 1179–1181.